International Journal of Thermophysics, Vol. 23, No. 5, September 2002 (© 2002)

Measurement of Thermal Expansion at High Temperature by a Transient Interferometric Technique[1]

P. Reiter[2] and E. Kaschnitz[2, 3]

A transient interferometric technique to measure the thermal expansion of pure metals and alloys during rapid heating is presented. The metallic specimen is resistively heated from room temperature to a high temperature close to melting within approximately 500 ms by the passage of a high electrical current pulse. The temperature of the specimen is measured and time resolved by a fast pyrometer; the thermal expansion is obtained by a high-speed laser-interferometer. The device used is a modified polarized-beam Michelson-type interferometer with a phase-quadrature detector that distinguishes between expansion and contraction. Details of its principle, the construction, adjustment, and operation are described. In addition, thermal expansion measurements performed on molybdenum and tungsten standard reference materials (SRMs) are presented and compared with results obtained by other researchers.

KEY WORDS: high temperature; interferometry; molybdenum; thermal expansion; tungsten.

1. INTRODUCTION

Measurements of thermophysical properties of metals and alloys in the high temperature range are prone to error due to experimental difficulties, such as heat losses due to radiation, convection or heat flux, chemical reactions of the specimen with the containment, and evaporation of the specimen material. It is possible to overcome many of these problems by performing transient heating experiments with rapid heating of the specimen. A convenient method for pulse heating metals and alloys is resistive self-heating, where a high-current pulse is used to heat the specimen. The

[1] Paper presented at the Sixth International Workshop on Subsecond Thermophysics, September 26–28, 2001, Leoben, Austria.

[2] Österreichisches Gießerei-Institut, Parkstraße 21, 8700 Leoben, Austria.

[3] To whom correspondence should be addressed. E-mail: kaschnitz.ogi@unileoben.ac.at

0195-928X/02/0900-1327/0 © 2002 Plenum Publishing Corporation

time dependence of the specimen temperature is obtained by measuring the emitted thermal radiation by a high-speed pyrometer.

In this paper, a fast polarized-beam Michelson-type interferometer for the measurement of the thermal expansion of a pulse-heated metallic specimen is presented. It uses a phase-quadrature detector that allows expansion and contraction to be distinguished.

2. EXPERIMENTAL

2.1. Pulse Heating System

A description of the construction and operation of the pulse-heating system and the single-wavelength high-speed pyrometer is given in earlier publications [1, 2]. By the passage of a high current, the specimen is pulse-heated from room temperature to a high temperature close to melting in less than 500 ms. The specimen temperature is measured by a fast single-wavelength pyrometer every 50 μs. The effective wavelength of its interference filter is 902 nm in the temperature range 1200 to 2300 K and 649 nm in the range 1800 to 3800 K, each with a bandwidth (FWHM) of 20 nm. The pyrometer is calibrated by means of two tungsten strip lamps (vacuum and gas filled) covering temperature ranges 1000 to 1700 K and 1700 to 2600 K, respectively.

2.2. Specimen

The heated specimen is a tube with a length of approximately 75 mm, an outer diameter of 6.4 mm, and an inner diameter of 5.3 mm (Fig. 1).

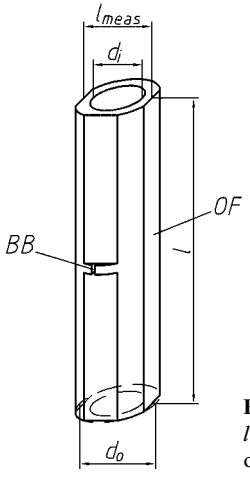

Fig. 1. Specimen shape. d_o, outer diameter; d_i, inner diameter; l_{meas}, measurement length; l, total length; BB, blackbody hole; OF, optical flat at one side.

The specimen has two polished parallel flat surfaces that are used as mirrors for the interferometric measurements. A rectangular hole of 0.5×1.0 mm is machined into the wall of the specimen to approximate blackbody conditions for the temperature measurement. Material is removed over the remaining length to achieve a constant cross section over the full length.

2.3. Interferometer

The interferometer is a high-speed modified Michelson-type interferometer similar to the one developed by Miiller and Cezairliyan [3]. A schematic diagram of the interferometer is given in Fig. 2. The linear polarized beam from the helium-neon laser is directed by the mirrors M_1 and M_2 to the polarizing beam splitter BS_1, and split into two orthogonal polarized beams. The transmitted (measurement) beam is *p*-polarized when it leaves BS_1. The principal axis of the quarter-wave plate Q_1 is oriented at $\pi/4$ to the plane of the interferometer. By passing Q_1, the polarization state of the measurement beam is changed from linear to circular. Thereafter, the beam is focused on one of the polished surfaces of the specimen S by the lens L_1, where it is reflected, and the sense of circular polarization is reversed. Passing the quarter-wave plate Q_1 again, the polarization state is switched back from circular polarization to linear *s*-polarization. Now the measurement beam is reflected by the pentaprism PP_1 and the plane mirror M_3.

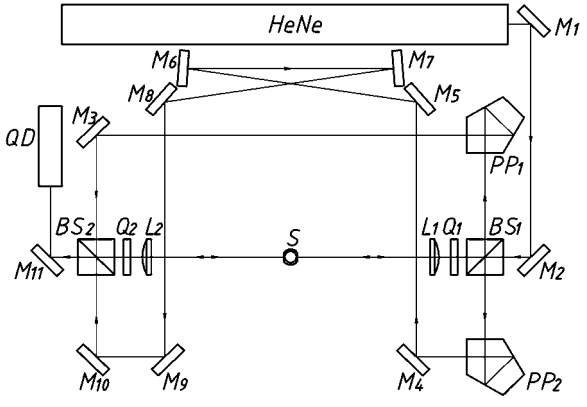

Fig. 2. Schematic diagram of the modified polarized beam Michelson-type interferometer. S, specimen; M_1-M_{11}, flat mirrors; BS_1, BS_2, polarizing beam splitters; Q_1, Q_2, quarter-wave plates; L_1, L_2, lenses; PP_1, PP_2, pentaprisms; HeNe, helium-neon laser; QD, phase-quadrature detector.

The beam is *s*-polarized and therefore reflected by BS_2. The elements BS_2, Q_2 and L_2 serve in the same manner as BS_1, Q_1, and L_1, so the measurement beam leaves BS_2 towards M_{11}, being *p*-polarized.

The second (reference) beam emerging from beam splitter BS_1 is *s*-polarized. It is reflected by pentaprism PP_2, the mirrors M_4 to M_{10} and beam splitter BS_2. The measurement beam and the reference beam leaving BS_2 are co-linear, and their polarization angles are orthogonal. The phase shift between these beams changes, as the optical path of the measurement beam changes due to thermal expansion of the specimen. A translational movement of the specimen, which may be generated by forces due to the high current pulse, has no influence on the difference in optical path length between the two beams.

The lenses L_1 and L_2 together with the pentaprism PP_1 minimize the sensitivity of the interferometer to possible rotational motion of the specimen during heating [3]. Since the polished surfaces of the specimen coincide with the focal planes of the lenses L_1 and L_2, an angular deviation of the reflected beam leads to a lateral displacement of the measurement beam after passing L_1. If the number of reflections of the measurement beam between the beam splitters BS_1 and BS_2 were even, the measurement beam would suffer a second lateral displacement at the second specimen surface adding to the first one. In order to keep the number of reflections odd, a pentaprism (PP_1) is used to reflect the measurement beam, and the two lateral offsets compensate each other. PP_2 is also a pentaprism to make sure that the number of reflections of the measurement and reference beams have the same parity. Since the coherence length of the He-Ne laser used is only a few centimeters, the plane mirrors M_5 through M_8 are used to match the optical path length of the reference beam and the measurement beam.

A phase-quadrature detector is used to detect the phase shift between the two beams emerging from the interferometer (Fig. 3). This detector consists of a beam expander (BE), an interference filter (IF) with a center wavelength of 632.8 nm, a quarter-wave plate (Q_3), a four-quadrant analyzer (FA), and a four-quadrant photodiode (PD). The narrow band interference filter minimizes the background thermal radiation from the specimen. The principal axis of the quarter-wave plate is adjusted to an angle of $\pi/4$ to the plane of the interferometer.

The entire interferometric setup is mounted on an optical table to minimize vibrations. All measurement signals (thermal radiation intensities,

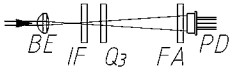

Fig. 3. Schematic diagram of phase-quadrature detector. BE, beam expander; IF, interference filter; Q_3, quarter-wave plate; FA, four-quadrant analyzer; PD, four-quadrant photodiode.

four-quadrant photodiode signals) are measured by a 16-bit data acquisition system providing simultaneous sampling of all channels with a sampling rate of 20 $kS \cdot s^{-1}$.

3. DATA REDUCTION

The two emerging beams from the interferometer entering the phase-quadrature detector can be described as plane waves,

$$\mathbf{E}_{\text{out}} = \begin{pmatrix} E_M e^{i\varphi_M} \\ E_R e^{i\varphi_R} \end{pmatrix} \tag{1}$$

where $\mathbf{E}$ is the electrical field strength, φ is the phase, subscript M is the measurement beam, and subscript R is the reference beam. The influence of a quarter-wave plate is described by a Jones Matrix $\mathbf{J}_{\lambda/4,\ 45^\circ}$. After passing the quarter-wave plate, the electrical field strength is altered

$$\begin{aligned} \mathbf{E}_{\text{out},2} = \mathbf{J}_{\lambda/4,\,45^\circ}\mathbf{E}_{\text{out}} &= \frac{1}{\sqrt{2}}\begin{pmatrix} 1 & i \\ i & 1 \end{pmatrix}\begin{pmatrix} E_M e^{i\varphi_M} \\ E_R e^{i\varphi_R} \end{pmatrix} \\ &= \begin{pmatrix} E_M e^{i\varphi_M} + iE_R e^{i\varphi_R} \\ iE_M e^{i\varphi_M} + E_R e^{i\varphi_R} \end{pmatrix} \\ &= \begin{pmatrix} E_M e^{i\varphi_M} + E_R e^{i(\varphi_R+\pi/2)} \\ E_M e^{i(\varphi_M+\pi/2)} + E_R e^{i\varphi_R} \end{pmatrix} \end{aligned} \tag{2}$$

and passes the four-quadrant analyzer, arranged in four sectors with their polarization axes at 0, $\pi/4$, $\pi/2$, and $3\pi/4$, giving the following field strengths at each sector (subsection *a* to *d*)

$$\begin{aligned} \mathbf{E}_1 = \mathbf{J}_{0^\circ}\mathbf{E}_{\text{out},2} &= \begin{pmatrix} 1 & 0 \\ 0 & 0 \end{pmatrix}\begin{pmatrix} E_M e^{i\varphi_M} + E_R e^{i(\varphi_R+\pi/2)} \\ E_M e^{i(\varphi_M+\pi/2)} + E_R e^{i\varphi_R} \end{pmatrix} \\ &= \begin{pmatrix} E_M e^{i\varphi_M} + E_R e^{i(\varphi_R+\pi/2)} \\ 0 \end{pmatrix} \end{aligned} \tag{3a}$$

$$\begin{aligned} \mathbf{E}_2 = \mathbf{J}_{45^\circ}\mathbf{E}_{\text{out},2} &= \frac{1}{2}\begin{pmatrix} 1 & 1 \\ 1 & 1 \end{pmatrix}\begin{pmatrix} E_M e^{i\varphi_M} + E_R e^{i(\varphi_R+\pi/2)} \\ E_M e^{i(\varphi_M+\pi/2)} + E_R e^{i\varphi_R} \end{pmatrix} \\ &= \frac{1}{\sqrt{2}}\begin{pmatrix} E_M e^{i(\varphi_M+\pi/4)} + E_R e^{i(\varphi_R+\pi/4)} \\ E_M e^{i(\varphi_M+\pi/4)} + E_R e^{i(\varphi_R+\pi/4)} \end{pmatrix} \end{aligned} \tag{3b}$$

$$\mathbf{E}_3 = \mathbf{J}_{90^\circ}\mathbf{E}_{\text{out},2} = \begin{pmatrix} 0 & 0 \\ 0 & 1 \end{pmatrix} \begin{pmatrix} E_M e^{i\varphi_M} + E_R e^{i(\varphi_R + \pi/2)} \\ E_M e^{i(\varphi_M + \pi/2)} + E_R e^{i\varphi_R} \end{pmatrix}$$

$$= \begin{pmatrix} 0 \\ E_M e^{i(\varphi_M + \pi/2)} + E_R e^{i\varphi_R} \end{pmatrix} \tag{3c}$$

$$\mathbf{E}_4 = \mathbf{J}_{-45^\circ}\mathbf{E}_{\text{out},2} = \frac{1}{2}\begin{pmatrix} 1 & -1 \\ -1 & 1 \end{pmatrix} \begin{pmatrix} E_M e^{i\varphi_M} + E_R e^{i(\varphi_R + \pi/2)} \\ E_M e^{i(\varphi_M + \pi/2)} + E_R e^{i\varphi_R} \end{pmatrix}$$

$$= \frac{1}{\sqrt{2}}\begin{pmatrix} -E_M e^{i(\varphi_M - \pi/4)} + E_R e^{i(\varphi_R - \pi/4)} \\ E_M e^{i(\varphi_M - \pi/4)} - E_R e^{i(\varphi_R - \pi/4)} \end{pmatrix} \tag{3d}$$

where $\mathbf{J}_{0^\circ}$, $\mathbf{J}_{45^\circ}$, $\mathbf{J}_{90^\circ}$, and $\mathbf{J}_{-45^\circ}$, are the Jones matrices describing the four-quadrant analyzer. Squaring the field strengths with the phase difference between measurement and reference beams $\Delta\varphi$ given by

$$\Delta\varphi = \varphi_M - \varphi_R \tag{4}$$

results in intensities I_1 through I_4,

$$\begin{aligned} I_1 &= E_M^2 + E_R^2 + 2E_M E_R \sin \Delta\varphi \\ I_2 &= E_M^2 + E_R^2 + 2E_M E_R \cos \Delta\varphi \\ I_3 &= E_M^2 + E_R^2 - 2E_M E_R \sin \Delta\varphi \\ I_4 &= E_M^2 + E_R^2 - 2E_M E_R \cos \Delta\varphi \end{aligned} \tag{5}$$

which are converted to voltages U_1 to U_4 by the four-quadrant photodiode. The photodiode signals are proportional to the individual intensities by a factor k, and the phase difference is obtained by the ratio of the differences of the opposite detector signals,

$$\frac{U_1 - U_3}{U_2 - U_4} = \frac{4kE_M E_R \sin \Delta\varphi}{4kE_M E_R \cos \Delta\varphi} = \frac{\sin \Delta\varphi}{\cos \Delta\varphi} = \tan \Delta\varphi \tag{6}$$

A case distinction is made to extend the phase-difference angle between $-\pi$ and π

$$(U_1 - U_3 \geqslant 0) \cap (U_2 - U_4 > 0) \Leftrightarrow \text{Quadrant 1} \Rightarrow \Delta\varphi = \arctan \frac{U_1 - U_3}{U_2 - U_4}$$

$$(U_1 - U_3 \geqslant 0) \cap (U_2 - U_4 < 0) \Leftrightarrow \text{Quadrant 2} \Rightarrow \Delta\varphi = \arctan \frac{U_1 - U_3}{U_2 - U_4} + \pi$$

$$(U_1 - U_3 < 0) \cap (U_2 - U_4 < 0) \Leftrightarrow \text{Quadrant 3} \Rightarrow \Delta\varphi = \arctan \frac{U_1 - U_3}{U_2 - U_4} - \pi$$

$$(U_1 - U_3 < 0) \cap (U_2 - U_4 > 0) \Leftrightarrow \text{Quadrant 4} \Rightarrow \Delta\varphi = \arctan \frac{U_1 - U_3}{U_2 - U_4}$$

$$(U_1 - U_3 > 0) \cap (U_2 - U_4 = 0) \qquad \Rightarrow \Delta\varphi = \frac{\pi}{2}$$

$$(U_1 - U_3 < 0) \cap (U_2 - U_4 = 0) \qquad \Rightarrow \Delta\varphi = -\frac{\pi}{2} \tag{7}$$

The measured phase difference as a function of time is obtained as a saw-tooth shaped curve oscillating between $-\pi$ and π. This function is phase unwrapped numerically. The thermal expansion of the specimen is obtained by

$$\Delta l_{T_i \to T}(T) = \lambda_{\text{Laser}} \frac{\Delta\varphi(T) - \Delta\varphi(T_i)}{2\pi} \tag{8}$$

where λ_{Laser} is the wavelength of the laser, $\Delta\varphi(T_i)$ is the initial phase difference, $\Delta\varphi(T)$ is the phase difference at the temperature T, and T_i is the initial temperature.

4. MEASUREMENTS

All measurements have been performed under high vacuum conditions. The signals of the four-quadrant analyzer are initially slightly disturbed and show deviations from the sinusoidal shape due to the rapid rise of the heating current (Fig. 4). A standardization algorithm is applied to scale the signals in order to compensate for different amplitudes of the signals.

The distance between the optical flats of the specimen, which are acting as mirrors, is measured by a precision micrometer at room temperature (293 K). The temperature of the specimen before the start of the measurement is obtained by a thermocouple mounted to the current clamps. A small correction for the deviation of the specimen temperature from the reference temperature T_0 has been applied.

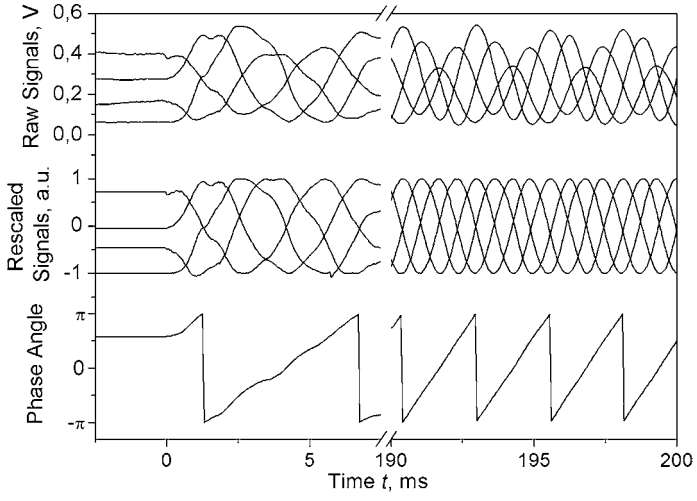

Fig. 4. Example of recorded raw signals of the phase-quadrature detector at the beginning and during the experiment, the re-scaled signals, and the obtained phase angle.

5. RESULTS

5.1. Molybdenum

A total of six pulse experiments in the temperature range 1000 to 2300 K on one specimen made of SRM 781 has been made. The deviation of the single experiments from the mean value is less than 0.5%. The results for the linear thermal expansion are shown in Table I. The least-

Table I. Linear Thermal Expansion of Molybdenum in the Temperature Range between 1000 and 2300 K (Reference temperature $T_0 = 293$ K)

T (K)	$\Delta l/l_0$ (%)	T (K)	$\Delta l/l_0$ (%)	T (K)	$\Delta l/l_0$ (%)
1000	0.416	1450	0.720	1900	1.077
1050	0.448	1500	0.757	1950	1.121
1100	0.480	1550	0.794	2000	1.166
1150	0.513	1600	0.832	2050	1.212
1200	0.547	1650	0.871	2100	1.260
1250	0.580	1700	0.910	2150	1.308
1300	0.615	1750	0.950	2200	1.358
1350	0.649	1800	0.992	2250	1.409
1400	0.685	1850	1.034	2300	1.461

Table II. Linear Thermal Expansion of Tungsten in the Temperature Range between 1000 and 2300 K (Reference temperature $T_0 = 293$ K)

T (K)	$\Delta l/l_0$ (%)	T (K)	$\Delta l/l_0$ (%)	T (K)	$\Delta l/l_0$ (%)
1000	0.344	1900	0.856	2800	1.506
1100	0.399	2000	0.919	2900	1.593
1200	0.454	2100	0.984	3000	1.683
1300	0.509	2200	1.050	3100	1.778
1400	0.564	2300	1.119	3200	1.876
1500	0.621	2400	1.191	3300	1.979
1600	0.678	2500	1.265	3400	2.087
1700	0.736	2600	1.342	3500	2.199
1800	0.795	2700	1.422		

squares fit to the experimental data of the thermal expansion in the temperature range 1200 to 2300 K results in

$$\frac{\Delta l_{T_0 \to T}(T)}{l_0} = -0.2300 + 7.0393 \times 10^{-4} T - 1.1386 \times 10^{-7} T^2 + 5.5453 \times 10^{-11} T^3$$

$$\text{where} \quad \frac{\Delta l_{T_0 \to T}(T)}{l_0} \quad \text{is in \% and } T_0 = 293 \text{ K} \tag{9}$$

5.2. Tungsten

A total of 15 pulse experiments in the temperature range 1000 to 3500 K on three specimens made of SRM 737 has been made. The deviation of the single experiments from the mean value is less than 0.5%. Results for the linear thermal expansion are shown in Table II.

The least-squares fit to the experimental data of the thermal expansion in the temperature range 1200 to 3500 K results in

$$\frac{\Delta l_{T_0 \to T}(T)}{l_0} = -0.2430 + 6.6026 \times 10^{-4} T - 1.0671 \times 10^{-7} T^2 + 3.355 \times 10^{-11} T^3$$

$$\text{where} \quad \frac{\Delta l_{T_0 \to T}(T)}{l_0} \quad \text{is in \% and } T_0 = 293 \text{ K} \tag{10}$$

6. ESTIMATE OF UNCERTAINTIES

An analysis of sources of uncertainties for the linear thermal expansion is given in Table III. The major contribution to the uncertainty is the

Table III. Summary of Uncertainties of the Thermal Expansion of Tungsten at 2600 K

Source of uncertainty	Value	Uncertainty	Sensitivity coefficient	Contribution to total uncertainty
Outer influences	0.00–	0.25–	5.20×10^{-3}%	0.0013%
Nonlinearity	0.00–	0.25–	5.20×10^{-3}%	0.0013%
Measurement length	6.09 mm	0.01 mm	2.20×10^{-1}%·(mm)$^{-1}$	0.0022%
Expansivity at initial temperature	450×10^{-8} K^{-1}	9×10^{-8} K^{-1}	6.20×10^{2}%·K	0.0056%
Uncertainty of initial temperature	299.2 K	1.0 K	4.50×10^{-4} %·K^{-1}	0.0005%
Rotational movements	0.0°	0.2°	} [a]	0.0293%
Misalignment of beams	0.0 mm	−0.5 mm	} [a]	
Axial nonparallelism of flats	0.00 mm	0.01 mm	1.64×10^{-1} %·(mm)$^{-1}$	0.0016%
Temperature	2600 K	6 K	5.47×10^{-4} %·K^{-1}	0.0034%
Total uncertainty				0.0302%
Expanded total uncertainty				**0.0604%**

[a] Since rotational movement and misalignment of the measurement beams produce a common contribution to the total uncertainty, no sensitivity coefficients are given.

influence of possible rotational movements during pulse heating. A more detailed description of this specific influence is presented in Ref. 3. The expanded total uncertainty in $\Delta l/l_0$ (expressed in %) for tungsten at 2600 K is 0.0604%, which corresponds to a relative uncertainty of 4.5%.

7. DISCUSSION

A comparison of the results obtained in this work with those of other research groups is given in Figs. 5. and 6. Miiller and Cezairliyan [4, 5] used a transient interferometric technique that is very similar to the one described in this paper. Petukhov et al. [6, 7] used a steady-state comparator technique, Suh et al. [8] presented results measured with a dilatometer, and the results of Waseda et al. [9] were obtained by X-ray diffraction. In the studies of Fokin and Chekhovskoi [10] and White and Roberts [11], several earlier results are analyzed and recommended values are given. Kirby [12] worked with a twin microscope method using specimens from three different suppliers. In Fig. 6 an average of those results of Ref. 12 is shown. Wang and Reeber [13] present a theoretical approach that takes the role of defects into account.

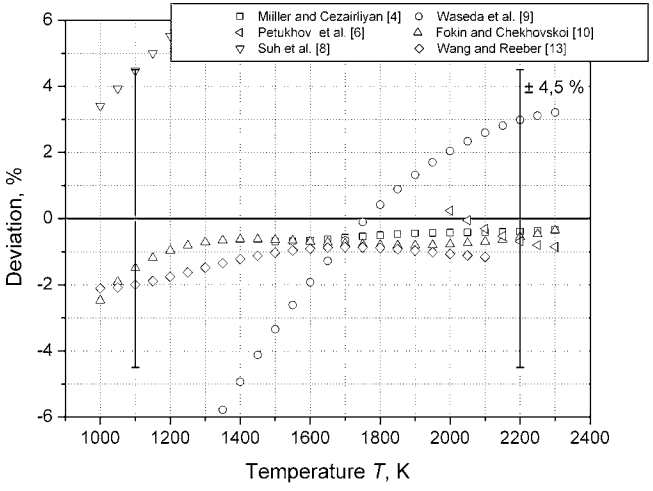

Fig. 5. Comparison of the linear thermal expansion of molybdenum obtained by other investigators with the present results. The error bars indicate the expanded relative uncertainty of the present work.

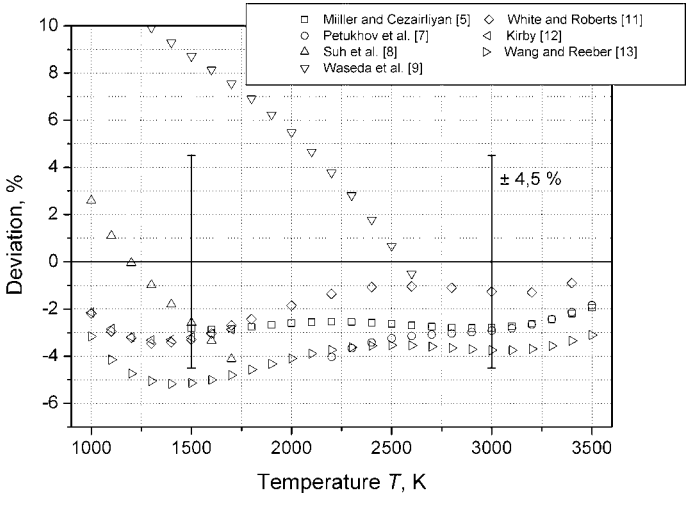

Fig. 6. Comparison of the linear thermal expansion of tungsten obtained by other investigators with the present results. The error bars indicate the expanded relative uncertainty of the present work.

ACKNOWLEDGMENT

This work was supported by the Fonds zur Förderung der wissenschaftlichen Forschung (FWF), Vienna, Austria under Contract No. P12804-PHY.

REFERENCES

1. P. Reiter and E. Kaschnitz, *High Temp.-High Press*, **33**:505 (2001).
2. E. Kaschnitz and P. Reiter, *J. Thermal Analysis Calorimetry* **64**:351 (2001).
3. A. P. Miiller and A. Cezairliyan, *Int. J. Thermophys.* **3**:259 (1982).
4. A. P. Miiller and A. Cezairliyan, *Int. J. Thermophys.* **6**:695 (1985).
5. A. P. Miiller and A. Cezairliyan, *Int. J. Thermophys.* **11**:619 (1990).
6. V. A. Petukhov, V. Ya. Chekhovskoi, and V. M. Zaichenko, *Translated from Teplofizika Vysokikh Temperatur* **14**:724 (1976).
7. V. A. Petukhov and V. Ya. Chekhovskoi, *High Temp.-High Press.* **4**:671 (1972).
8. In-Kook Suh, H. Ohta, and Y. Waseda, *J. Materials Science* **23**:757 (1988).
9. Y. Waseda, K. Hirata, and M. Ohtani, *High Temp.-High Press.* **7**:221 (1975).
10. L. R. Fokin and V. Ya. Chekhovskoi, *Translated from Teplofizika Vysokikh Temperatur* **29**:94 (1991).
11. G. K. White and R. B. Roberts, *High Temp.-High Press.* **15**:321 (1983).
12. R. K. Kirby, *High Temp.-High Press.* **4**:459 (1972).
13. K. Wang and R. R. Reeber, *Materials Science and Engineering* **R23**:101 (1998).